

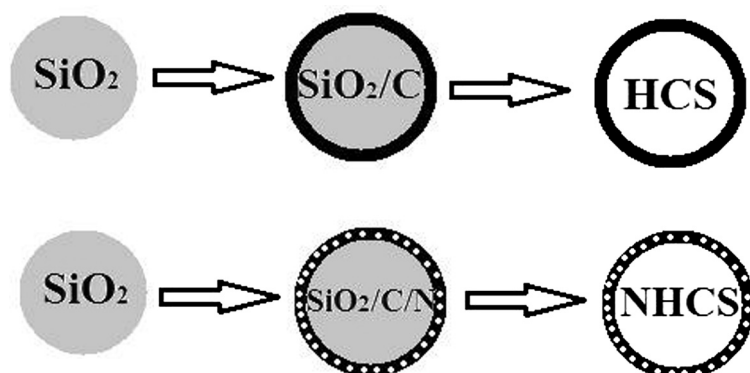


## Regular Article

## Facile synthesis N-doped hollow carbon spheres from spherical solid silica

K. Wenelska<sup>a,\*</sup>, A. Ottmann<sup>b,\*</sup>, D. Moszyński<sup>a</sup>, P. Schneider<sup>b</sup>, R. Klingeler<sup>b,c</sup>, E. Mijowska<sup>a</sup><sup>a</sup> *Nanomaterials Physicochemistry Department, Institute of Chemical and Environment Engineering, West Pomeranian University of Technology, al. Piastów 45, 70-322 Szczecin, Poland*<sup>b</sup> *Kirchhoff Institute of Physics, Heidelberg University, INF 227, 69120 Heidelberg, Germany*<sup>c</sup> *Centre for Advanced Materials (CAM), Heidelberg University, INF 225, 69120 Heidelberg, Germany*

## GRAPHICAL ABSTRACT



## ARTICLE INFO

## Article history:

Received 24 July 2017

Revised 18 September 2017

Accepted 3 October 2017

Available online 5 October 2017

## Keywords:

Hollow carbon spheres

Lithium ion batteries

Carbon materials

## ABSTRACT

Nitrogen-doped core/shell carbon nanospheres (NHCS) are prepared and their capability as an anode material in lithium-ion batteries is investigated. The synthesis methodology is based on a fast template route. The resulting molecular nanostructures are characterized by X-ray diffraction, transmission electron microscopy, thermal analysis, and nitrogen adsorption/desorption measurement as well as by cyclic voltammetry and galvanostatic cycling. The core/shell structure provides a rapid lithium transport pathway and boasts a highly reversible capacity. For undoped HCS the BET specific surface area is 623 m<sup>2</sup>/g which increases up to 1000 m<sup>2</sup>/g upon N-doping. While there is no significant effect of N-doping on the electrochemical performance at small scan rates, the doped NHCS shows better specific capacities than the pristine HCS at elevated rates. For instance, the discharge capacities in the 40th cycle, obtained at 1000 mA/g, amount to 170 mAh/g and 138 mAh/g for NHCS and HCS, respectively.

© 2017 Elsevier Inc. All rights reserved.

## 1. Introduction

Lithium-ion batteries with high-power, energy density and long life cycle are necessary for electric devices, mostly for electric vehi-

cles and other portable electric devices [1–4]. Due to the low kinetics limited by the slow solid-state lithium-ion diffusion their power density is generally low because of the large polarization at high charge–discharge rates [5,6]. The most popular material for the anodes in Li-ion batteries (LIB) is mainly carbon. Especially, graphite due to its high Coulombic efficiency, high theoretical capacity, stability, and safety [7]. A lot of research focuses on

\* Corresponding authors.

E-mail addresses: [kwenelska@zut.edu.pl](mailto:kwenelska@zut.edu.pl) (K. Wenelska), [alexander.ottmann@kip.uni-heidelberg.de](mailto:alexander.ottmann@kip.uni-heidelberg.de) (A. Ottmann).

discovery alternatives for graphite for new generation batteries more efficient by improving high energy density, good cycling and rate performance [8–10]. Therefore, different forms of carbon materials such as micro- to macroporous carbon materials [11–14], carbon nanotubes [15,16], nanofibers [17], and graphene [18–21] have been obtained as alternative anode materials to improve the energy density of LIB. A better storage capacity can be achieved for disordered carbon rather than graphitic carbon provides. Due to unique properties that the application of nanostructured electrode materials, in particular obtain mesoporous materials, is a good approach to improve the power density [22–25]. Materials with order pores have a better properties for example large surface area, which decrease the current density per unit surface area. Additionally the thin walls can reduce the length of the diffusion path. Furthermore this materials can facilitate ionic motion compared with another mesoporous carbon materials. Many researchers focus on obtain mesoporous electrode materials which can be used like anode material for electrode in LIB.

Porous carbon materials have been usually used as high surface area electrodes because characterized by low cost, good process ability, and high stability [5,6,26].

Because of the fact that their charge storage mechanism solely depends on the adsorption of electrolyte ions onto the electrode surface their electrochemical performance has been limited [27,28]. Recently, nitrogen [29,30] or boron [31,32] doped carbon materials have been prepared and used as alternative anode materials to obtain the Li storage capability. Advanced techniques and research show that for the lithium adsorption of N- and B-doped materials imply that B-doping decreases the Li adsorption energies, while N-doping increases the Li adsorption energies [33,34]. The most suitable for Li storage with a high storage capacity is carbon framework including the pyridinic carbon. For this structure N-doping has been is the most favorable. In comparison, nitrogen-doped porous carbons have raised attention as electrode materials for LIB due to their superior electrochemical properties. Nitrogen dopants presented new mechanism of charge storage known as pseudo-capacitance, in which through fast surface reaction the charge is stored [35,36].

Here, we report a simple synthesis route of hollow carbon nanospheres doped with nitrogen. The spheres were prepared based on the template method presented in [A11] and uses lysine as the nitrogen source. The detailed characterization of the structure and the morphology shows mesoporous spherical particles with high BET specific surface areas of up to  $\sim 1000 \text{ m}^2/\text{g}$ . Only at higher scan rates, the electrochemical performance of N-doped HCS is superior to the undoped material.

## 2. Experimental

**Synthesis of SiO<sub>2</sub> Spheres.** SiO<sub>2</sub> nanospheres were prepared by a modified Stober sol-gel process [37]. Briefly, tetraethylorthosilicate (TEOS) (1.5 mL) was added to a mixture of ethanol (50 mL) and concentrated ammonia (28 wt%, 2.5 mL). Then the solution was stirred for 24 h. Afterwards, 0.5 g of the solid product was separated by filtration, washed with ethanol, and dried in vacuum. Afterwards, SiO<sub>2</sub> spheres were pretreated to cover them with an external layer of carbon. The process involved reflux at 110 °C for 8 h in a mixture of 0.1 ml of (3-Aminopropyl)triethoxysilane (APTES), 100 ml of toluene and 0.3 g of silica spheres.

**Synthesis of SiO<sub>2</sub>@Carbon Hollow Spheres (HCS).** To get carbon coated SiO<sub>2</sub> spheres, the above-prepared material was dispersed in 16 mL of H<sub>2</sub>O, 4 mL of ethanol, and 0.4 g of glucose. Then, the mixture was heated at 190 °C for 36 h in an autoclave. After this reaction  $\sim 100 \text{ mg}$  of SiO<sub>2</sub>@C was obtained. The SiO<sub>2</sub> cores were thoroughly washed with hydrofluoric acid to remove the sil-

ica and obtain the reference material – pristine hollow carbon nanospheres (HCS).

**Synthesis of Carbon Hollow Spheres doped with Nitrogen (NHCS).** Silica spheres were dispersed in 16 mL of H<sub>2</sub>O, 4 mL of ethanol, 0.4 g of glucose and 0.2 g of lysine. Then, the mixture was heated at 190 °C for 36 h in an autoclave. After this reaction,  $\sim 100 \text{ mg}$  of SiO<sub>2</sub> coated by carbon shells doped with nitrogen (SiO<sub>2</sub>@NHCS) was obtained.

The SiO<sub>2</sub> cores were removed by washing with hydrofluoric acid to obtain the final product (NHCS).

**Characterization.** Raman scattering was conducted on a Renishaw micro-Raman spectrometer ( $\lambda = 720 \text{ nm}$ ). X-ray diffraction (XRD) was conducted on a Philips diffractometer using Cu K $\alpha$  radiation. The morphology of the samples was examined by a FEI Tecnai F30 transmission electron microscope (TEM) with a field emission gun operating at 200 kV. N<sub>2</sub> adsorption/desorption isotherms were acquired at liquid nitrogen temperature (77 K) using a Quantachrome instrument, and the specific surface area was calculated by the Brunauer Emmett Teller (BET) method. The pore size distribution was determined using the Barrett–Joyner–Halenda (BJH) method. Thermogravimetric analysis (TGA) was carried out on 10 mg samples using a DTA-Q600 SDT TA at a heating rate of 10 °C/min from room temperature to 900 °C under air. The X-ray photoelectron spectra were obtained using Al K $\alpha$  ( $h\nu = 1486.6 \text{ eV}$ ) radiation with a Prevac system equipped with Scienta SES 2002 electron energy analyzer operating at constant transmission energy ( $E_p = 50 \text{ eV}$ ).

**Electrochemical studies.** Electrochemical studies by means of cyclic voltammetry (CV) and galvanostatic cycling with potential limitation (GCPL) were carried out with Swagelok-type two-electrode cells (see [38]). The working electrodes were prepared by mixing the hollow carbon spheres, carbon black (Timcal), and polyvinylidene fluoride (PVDF, Solvay) binder at a weight ratio of 70:15:15 in N-methyl-2-pyrrolidone, and spreading the resulting slurry onto Cu plate current collectors. After successive drying (24 h at 100 °C,  $p < 5 \text{ mbar}$ ), mechanical pressing (10 MPa) and repeated drying, the cells were assembled in an argon atmosphere glovebox (O<sub>2</sub>, H<sub>2</sub>O < 2 ppm). A lithium foil disk (Sigma-Aldrich) was used as counter electrode and 200  $\mu\text{l}$  of a 1 M solution of LiPF<sub>6</sub> in 1:1 ethylene carbonate/dimethyl carbonate (Merck LP30) served as electrolyte. The measurements were performed on a VMP3 multichannel potentiostat (BioLogic) while the cells were held at 25 °C in a climate chamber.

## 3. Results and discussion

The morphologies of HCS and NHCS were characterized by transmission electron microscopy (TEM). The TEM images presented in Fig. 1 show that solid SiO<sub>2</sub> nanospheres obtained by the modified Stober sol-gel process are monodispersed and the mean diameter is ca. 100 nm with a size distribution of 10 nm (Fig. 1a, b). The SiO<sub>2</sub>@HCS and SiO<sub>2</sub>@NHCS spheres from hydrothermal reactions are shown in Fig. 1a' and b', respectively. In addition, the core-shell-structured silica templates and the corresponding HCS (a'') and NHCS (b'') are shown in the figure. The TEM images reveal that the resulting materials exhibit monodispersed spherical particles that are uniform in size. The thickness of the shells is  $\sim 10 \text{ nm}$  both for HCS and NHCS.

Fig. 2 shows the powder XRD patterns of the synthesized HCS and NHCS. The black line which is corresponding to the carbon spherical spheres exhibits strong and broad peaks at  $2\theta = 24.9^\circ$  and  $42^\circ$ . These peaks can be ascribed to graphitic carbon, which is correspondingly seen in the Raman spectra presented below. For HCS doped with nitrogen (red line), the intensity of the peak at  $24.9^\circ$  is much weaker as compared to HCS, and the peak at  $42^\circ$

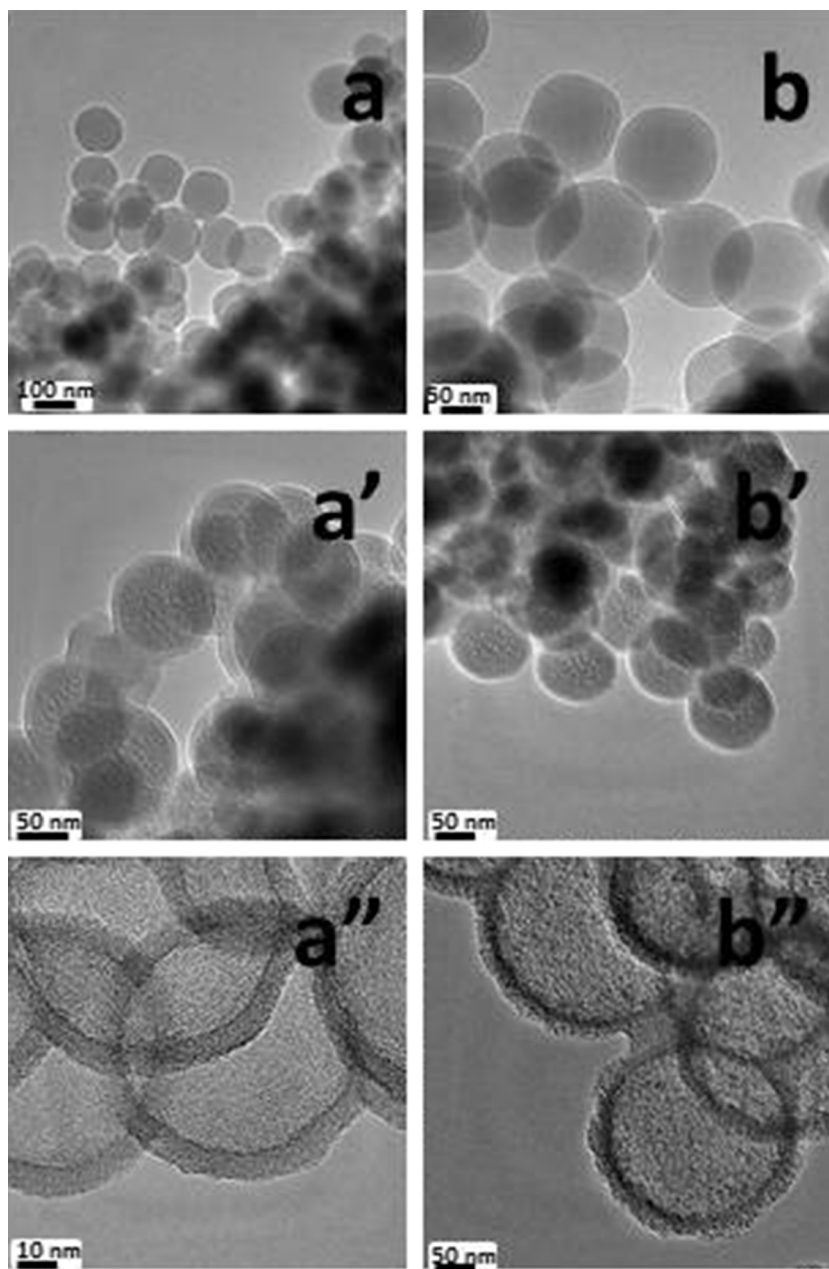


Fig. 1. TEM images of SiO<sub>2</sub> (a, b), SiO<sub>2</sub>@HCS (a'), SiO<sub>2</sub>@NHCS (b'), HCS (a''), and NHCS (b'').

has disappeared. These changes imply that the graphitic carbon structure of HCS has been deformed by N-doping.

TGA measurements in Fig. 3a impart information about the carbon content as well as the quality of the carbon spheres, because the oxidation temperature is affected by defects. Graphite starts to oxidize at 752 °C [39], but the TGA results in Fig. 3a show that NHCS is already oxidized above 365 °C and HCS above 415 °C. As the temperature is further increased, the weight loss increases rapidly until all of the carbon spheres are exhausted at approximately 495 °C for NHCS and 605 °C for HCS, respectively. The ash content of both HCS and NHCS was 0% (w/w), which implies that the materials have high purity.

Further information on the materials' structure and defects is obtained by Raman spectroscopy (Fig. 3b). The data show two distinct features in the wavelength regime under study which imply the presence of disordered graphitic materials. In particular, the

peak at 1593 cm<sup>-1</sup> (the so-called G-band) corresponds to the E<sub>2g</sub> mode of hexagonal graphite and is related to the vibration of the sp<sup>2</sup>-hybridized carbon atoms in a graphite layer. The observation of the G-band implies that the both materials are composed of graphitic carbon which is consistent with the TEM and the XRD results. The D-band at approximately 1359 cm<sup>-1</sup> is associated with the vibration of carbon atoms with dangling bonds in the plane with termination by disordered graphite. The intensity of the D-band measures the presence of such defects of the graphitic structure. In case of the pristine HCS, the IG/ID intensity ratio of the G- and D lines amounts to 0.9, indicating a high degree of graphitization. Note, that such a high crystallinity in general supports high electrical conductivity as desirable for application in Li-ion electrodes. Upon N-doped carbon, the relation of G-to D-band intensities slightly decreases which is consistent with the assumption that additional defects are formed in

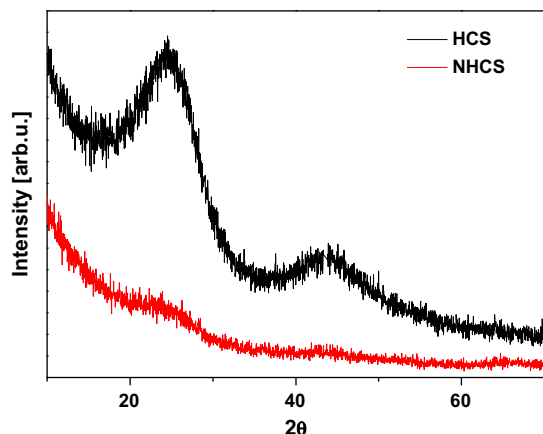


Fig. 2. Powder XRD patterns of HCS and NHCS.

the NHCS structures. In addition, the broadened peaks in XRD at  $2\Theta = 24.9$  and  $49^\circ$  and Raman spectroscopy for N-doped sample may be related to distortion in the C lattice due to the doping of nitrogen into HCS [40].

The Brunauer, Emmet, and Teller (BET) method has been used to measure the surface area of the final product. The  $N_2$  adsorption-desorption measurement shown in Fig. 4a exhibits that the large BET specific surface area of HCS further increases significantly

when they are doped with nitrogen. For HCS the BET specific surface area is  $623 \text{ m}^2/\text{g}$ . N-doped spheres with the same diameter exhibit a specific surface area of about  $1000 \text{ m}^2/\text{g}$ . The corresponding mesopore size distribution calculated by means of the BJH method from the adsorption branch reveals non-uniform pores centered at approximately 4, 5, 7 and 15 nm in case of the HCS, as shown in Fig. 4b. This result implies a mesoporous structure in the material.

The composition of the surface was examined by means of X-ray photoelectron spectroscopy. The presence of nitrogen is detected on the surface of both HCS and NHCS. The atomic concentration of N is estimated as 0.9 at.% and 3.5 at.%, respectively. Photoemission spectra of the N 1s transition are shown in Fig. 5. The main maximum of the N 1s peak is observed for both samples at a binding energy 400.5 eV. The component at 400.5 eV is the only one used for deconvolution of the N 1s line for the HCS sample. However, in case of NHCS another distinct component shows up in the spectra. Analysis of the spectrum as shown in Fig. 5 indicates the maximum of this additional component at a binding energy of 398.4 eV. Both peaks are symmetrical and exhibit a mixed Gaussian-Lorentzian profile. Additionally, a broad satellite shoulder is observed at a binding energy of 403.7 eV. The attribution of the chemical bonds of nitrogen to the experimentally observed XPS N 1s peaks is based on the review given in [41]. The component at a binding energy of 400.5 eV is attributed to the groups  $\text{NH}_x\text{C}=\text{O}$ , while the component at a binding energy of 398.4 eV comes from N–C bonds.

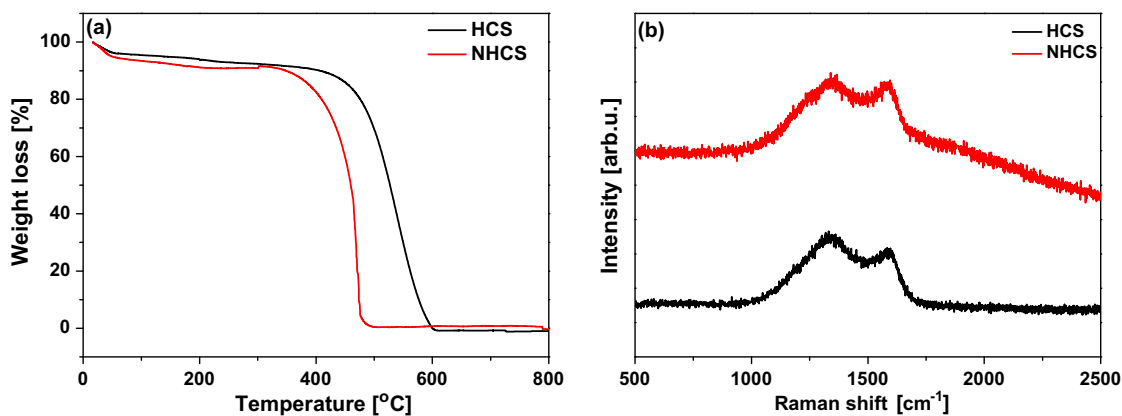


Fig. 3. (a) TGA profile and (b) Raman spectra of HCS and NHCS.

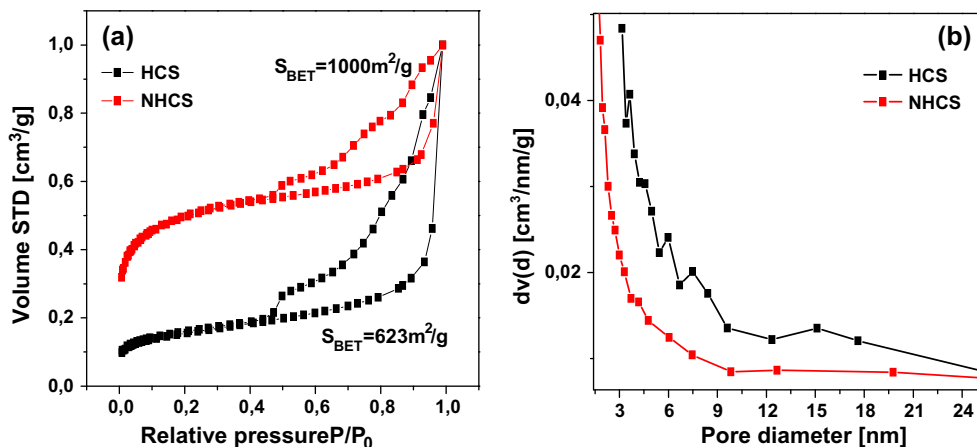


Fig. 4. (a) Nitrogen adsorption/desorption isotherms, and (b) corresponding pore size distribution profile of HCS and NHCS.

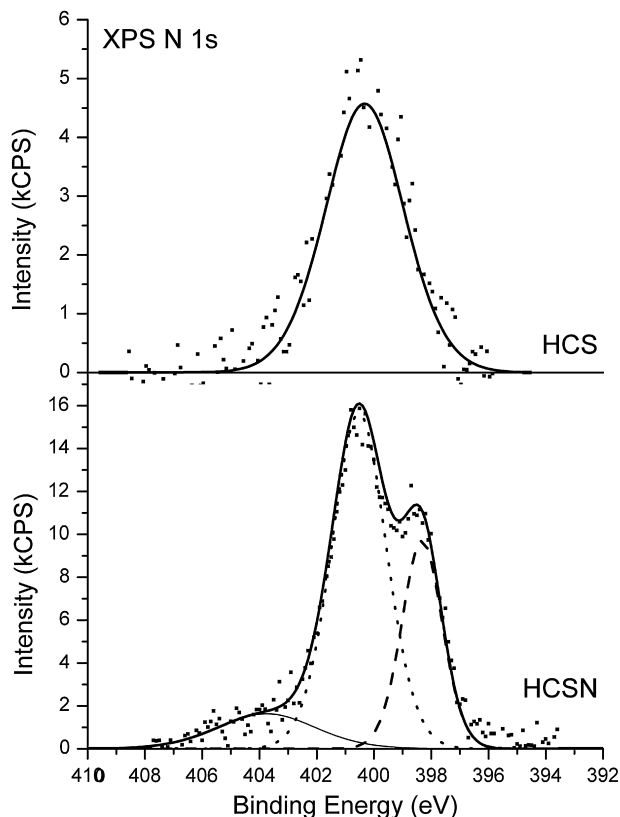


Fig. 5. XPS N 1s spectra of HCS and NHCS.

Cyclic voltammograms (CV) in the range of 0.01–3.0 V at a scan rate of 0.1 mV/s show very similar electrochemical activity of both HCS and NHCS (Fig. 6). During the initial cathodic half cycle two pronounced reductive features around 0.5 V and 0.01 V are observed. The former is attributed to the irreversible formation of a solid electrolyte interphase (SEI) [42–44], and is more distinct in case of the doped NHCS. The latter reduction peak at 0.01 V indicates the storage of  $\text{Li}^+$ -ions in the carbonaceous structures by means of intercalation and active sites, introduced at the surface or in pores [43,45]. Furthermore, two minor irreversible features occur at 1.15 V and 1.35 V (1st cycle), which may originate from

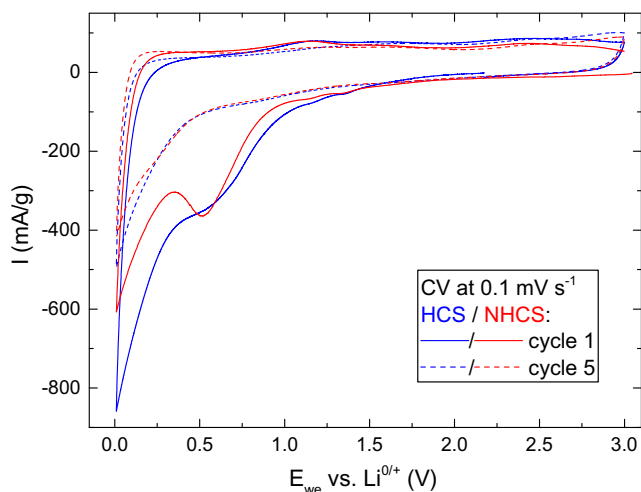


Fig. 6. Cyclic voltammograms of HCS and NHCS in the voltage range of 0.01–3.0 V, obtained at a scan rate of 0.1 mV/s.

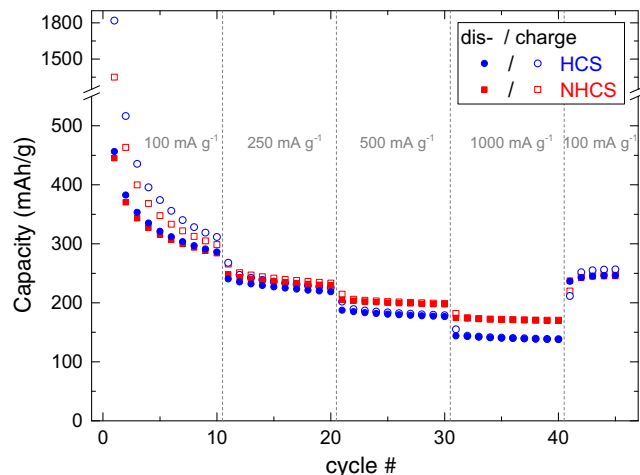


Fig. 7. Gravimetric specific capacities vs. cycle number of HCS and NHCS, at different scan rates between 100 and 1000 mAh/g. Open (full) symbols show the (dis)charge capacities.

the reduction of oxidative species on the surfaces of the HCS. The first anodic half cycle shows steady activity with two humps around 1.2 V and 2.4 V, corresponding to the delithiation of the HCS. In subsequent cycles, these features gradually level off and the oxidative activity towards 3.0 V increases. In the cathodic half cycles, the reduction peak around 0.01 V remains, but decreases in intensity as well. Overall, the gravimetric specific activity of the undoped HCS is slightly superior to NHCS. This fact is reflected in the first ten cycles of a GCPL at 100 mA/g between 0.01 V and 3.0 V (Fig. 7), which exhibits higher specific capacities for HCS than for NHCS. In both cases, the charge (lithiation) and discharge (delithiation) capacities significantly decrease from initially 1818/457 mAh/g and 1349/445 mAh/g to 311/286 mAh/g and 299/284 mAh/g, respectively, in cycle 10. The initial irreversibility from the first charge to discharge half cycle reflects the significant contribution of the SEI formation. Losses during subsequent cycling arise from a decline in general  $\text{Li}^+$  storage and extraction capability, as well indicated by decreasing peak intensities in the CVs (Fig. 6). The GCPL measurements were continued with a rate capability test featuring 10 cycles at 250, 500 and 1000 mA/g, respectively. While there is a noticeable capacity drop with each current step, the charge/discharge capacities stabilize with increasing cycle number. Furthermore, the doped NHCS show better specific capacities than the pristine HCS at elevated current rates of 500 mA/g and 1000 mA/g. For instance, the discharge capacities in the 40th cycle amount to 170 mAh/g and 138 mAh/g for NHCS and HCS, respectively. Going back to the initial charge/discharge current of 100 mA/g, the discharge capacities stabilize at 245 mAh/g (NHCS) and 246 mAh/g (HCS) in cycle 45, which in both cases is 86% of the ones in cycle 10. In summary, the N-doping of the HCS enhances the electrochemical performance only slightly, in particular compared to other studies [46–48]. The better rate capability could be facilitated by either improved conductivity [29,49] or higher specific surface area of the doped NHCS [50].

#### 4. Conclusions

Hollow carbon spheres with and without N-doping have been prepared using fast template synthesis. The source of nitrogen is lysine. Detailed characterization of the structure and the morphology shows monodisperse spherical particles. The hollow mesoporous structures have shells of about 10 nm thickness. While the Raman data of both materials are very similar and show no significant differences in the G- and D-bands, XRD and TGA imply

graphitic carbon in HCS and clearly lower crystallinity in NHCS. For HCS the BET specific surface area is 623 m<sup>2</sup>/g which increases up to 1000 m<sup>2</sup>/g upon N-doping. In contrast to N-doping in other carbon nanostructures, the electrochemical performance at small scan rates is similar. However, at elevated current rates, the doped NHCS show better specific capacities than the pristine HCS. For instance, the discharge capacities in the 40th cycle, obtained at 1000 mA/g, amount to 170 mAh/g and 138 mAh/g for NHCS and HCS, respectively. In summary, the N-doping of the HCS enhances the electrochemical performance only slightly.

### Acknowledgments

The authors are grateful for the financial support of National Science Centre, Poland PRELUDIUM 6-UMO-2013/11/N/ST8/00651 and by the German Academic Exchange Service DAAD (PPP project no. 56269175). AO and RK acknowledge support by the NanoTech-Initiative of the Baden-Württemberg-Stiftung (Project CT3: Nanostorage).

### References

- [1] M.S. Whittingham, *Chem. Rev.* 104 (2004) 4271.
- [2] B. Scrosati, *Nature* 373 (1995) 557–558.
- [3] T. Wen, W. Chen, *Power Sources* 92 (2) (2001) 139–148.
- [4] J. Luo, Y. Wang, H. Xiong, Y. Xia, *Chem. Mater.* 19 (19) (2007).
- [5] S.K. Sharma, M.-S. Kim, D.Y. Kim, J.-S. Yu, *Electrochim. Acta* 87 (2013) 872–879.
- [6] B. Fang, M.-S. Kim, J.H. Kim, J.-S. Yu, *Acc. Chem. Res.* 46 (2013) 1397–1406.
- [7] Y. Mao, H. Duan, B. Xu, L. Zhang, Y. Hu, C. Zhao, Z. Wang, L. Chena, Y. Yang, *Energy Environ. Sci.* 5 (2012) 7950–7955.
- [8] N.K. Chaudhari, M.-S. Kim, J.-S. Yu, *Electrochim. Acta* 114 (2013) 60–67.
- [9] K. Tokumitsu, H. Fujimoto, A. Mabuchi, T. Kasuh, *Carbon* 37 (1999) 1599–1605.
- [10] B. Fang, M.-S. Kim, J.H. Kim, S. Lim, J.-S. Yu, *J. Mater. Chem.* 20 (2010) 10253–10259.
- [11] J.S. Sakamoto, B. Dunn, *J. Mater. Chem.* 12 (2002) 2859–2861.
- [12] K.T. Lee, Y.S. Jung, S.M. Oh, *J. Am. Chem. Soc.* 125 (2003) 5652–5653.
- [13] M. Yoshio, H. Wang, K. Fukuda, *Angew. Chem., Int. Ed.* 42 (2003) 4203–4206.
- [14] M.-S. Kim, B. Fang, J.H. Kim, D. Yang, Y.K. Kim, T.S. Bae, J.-S. Yu, *J. Mater. Chem.* 21 (2011) 19362–19367.
- [15] S.W. Lee, N. Yabuuchi, B.M. Gallant, S. Chen, B.S. Kim, P.T. Hammond, Y. Shao-Horn, *Nat. Nanotechnol.* 5 (2010) 531–537.
- [16] B. Gao, A. Kleinhammes, X.P. Tang, C. Bower, L. Fleming, Y. Wu, O. Zhou, *Chem. Phys. Lett.* 307 (1999) 153–157.
- [17] B.S. Lee, S.B. Son, K.M. Park, W.R. Yu, K.H. Oh, S.H. Lee, *J. Power Sources* 199 (2012) 53–60.
- [18] E. Yoo, J. Kim, E. Hosono, H.-S. Zhou, T. Kudo, I. Honma, *Letter* 8 (2008) 2277–2282.
- [19] S.D.M. Brown, A. Jorio, M.S. Dresselhaus, G. Dresselhaus, *Phys. Rev. B* 64 (2001) 073403.
- [20] M. Liang, L. Zhi, *J. Mater. Chem.* 19 (2009) 5871–5878.
- [21] P. Lian, X. Zhu, S. Liang, Z. Li, W. Yang, H. Wang, *Electrochim. Acta* 55 (2010) 3909–3914.
- [22] H. Li, X. Wu, L.Q. Chen, X.J. Huang, *Solid State Ionics* 149 (2003) 185.
- [23] H. Li, L.H. Shi, W. Lu, X.J. Huang, L.Q. Chen, *J. Electrochem. Soc.* 148 (2001) 915.
- [24] S.S. Zhang, M.S. Ding, K. Xu, J. Jow, *Electrochem. Solid-State Lett.* 4 (2001) A206.
- [25] Z. Li, A. Ottmann, E. Thauer, C. Neef, H. Sai, Q. Sun, K. Cendrowski, H.-P. Meyer, Y. Vaynzof, E. Mijowska, J. Xiang, R. Klingeler, *RSC Adv.* 6 (2016) 76084–76092.
- [26] J.M. Tarascon, M. Armand, *Nature* 41 (4) (2001) 359–367.
- [27] E. Frackowiak, F. Beguin, *Carbon* 39 (2001) 937–950.
- [28] H.M. Jeong, J.W. Lee, W.H. Shin, Y.J. Choi, H.J. Shin, J.K. Kang, J.W. Choi, *Nano Lett.* 11 (2011) 2472–2477.
- [29] Z.S. Wu, W. Ren, L. Xu, F. Li, H.M. Cheng, *ACS Nano* 5 (2011) 5463–5471.
- [30] P. Han, Y. Yue, L. Zhang, H. Xu, Z. Liu, K. Zhang, C. Zhang, S. Dong, W. Ma, G. Cui, *Carbon* 50 (2012) 1355–1362.
- [31] L.G. Bulusheva, A.V. Okotrub, A.G. Kurennya, X. Chen, H. Song, *Carbon* 49 (2011) 4013–4023.
- [32] D.H. Wu, Y.F. Li, Z. Zhou, *Theor. Chem. Acc.* 130 (2011) 209–213.
- [33] X. Deng, L. Mammen, H.J. Butt, D. Vollmer, *Science* 335 (2012) 67–70.
- [34] Dh. Bhattacharjya, H.-Y. Park, M. Kim, H. Choi, S.N. Inamdar, J. Yu, *Langmuir* 30 (2014) 318–324.
- [35] H.D. Kodama, M. Shiraiishi, S. Hatori, H. Zhu, Z.H. Lu, *Adv. Funct. Mater.* 19 (2009) 1800–1809.
- [36] J. Jeon, R. Sharma, P. Meduri, B.W. Arey, H.T. Schaefer, J.L. Lutkenhaus, J.P. Lemmon, P.K. Thallapally, M.I. Nandasiri, B.P. McGrail, S.K. Nune, *ACS Appl. Mater. Interfaces* 6 (2014) 7214–7222.
- [37] W.J. Stober, *Colloid Interface Sci.* 26 (1968) 62–69.
- [38] C. Jähne, C. Neef, C. Koo, H.-P. Meyer, R. Klingeler, *J. Mater. Chem. A* 1 (2013) 2856–2862.
- [39] X. Chen, K. Kierzek, K. Wilgosz, J. Machnikowski, J. Gong, J. Feng, T. Tang, R.J. Kalenczuk, H. Chen, P.K. Chu, E. Mijowska, *J. Power Sources* 216 (2012) 475–481.
- [40] C. Di Valentin, G. Pacchioni, A. Selloni, S. Livraghi, E. Giamello, *J. Phys. Chem. B* 109 (2005) 11414–11419.
- [41] N. Graf, E. Yegen, T. Gross, A. Lippitz, W. Weigel, S. Krakert, A. Terfort, W.E. Unger, *Surf. Sci.* 18 (2009) 2849–2860.
- [42] D. Aurbach, Y. Ein-Eli, B. Markovskiy, A. Zaban, S. Luski, Y. Carmeli, H. Yamin, *J. Electrochem. Soc.* 142 (1995) 2882.
- [43] N.A. Kaskhedikar, J. Maier, *Adv. Mater.* 21 (2009) 2664.
- [44] K. Wenelska, A. Ottmann, P. Schneider, E. Thauer, R. Klingeler, E. Mijowska, *Energy* 103 (2016) 100–106.
- [45] S. Yang, X. Feng, L. Zhi, Q. Cao, J. Maier, K. Mullen, *Adv. Mater. (Deerfield Beach, Fla.)* 22 (2010) 838–842.
- [46] K. Zhang, X. Li, J. Liang, Y. Zhu, L. Hu, Q. Cheng, C. Guo, N. Lin, Y. Qian, *Electrochim. Acta* 155 (2015) 174.
- [47] F. Su, X.S. Zhao, Y. Wang, L. Wang, J.Y. Lee, *J. Mater. Chem.* 16 (2006) 4413.
- [48] Y. Wen, B. Wang, B. Luo, L. Wang, *Eur. J. Inorg. Chem.* 20 (2016) 2051.
- [49] Z.R. Ismagilov, A.E. Shalagina, O.Y. Podyacheva, A.V. Ischenko, L.S. Kibis, A.I. Boronin, Y.A. Chesalov, D.I. Kochubey, A.I. Romanenko, O.B. Anikeeva, T.I. Buryakov, E.N. Tkachev, *Carbon* 47 (2009) 1922–1929.
- [50] L. Qie, W.-M. Chen, Z.-H. Wang, Q.-G. Shao, X. Li, L.-X. Yuan, X.-L. Hu, W.-X. Zhang, Y.-H. Huang, *Adv. Mater. (Deerfield Beach, Fla.)* 24 (2012) 2047.